MedCave Publications
Inviting Scientific Discovery

Medcave Journal of Environmental Science & Technology

MedCave Publications

Research Article

Open Access

On Similarity of Seismo Magentic Power Density and Capillary Pressure Fractal Dimension for Characterizing Shajara Reservoirs of the Permo-Carboniferous Shajara Formation, Saudi Arabia

Khalid Elyas Mohamed Elameen Alkhidir*

Department of Petroleum and Natural Gas Engineering, King Saud University, Saudi Arabia

Corresponding Author: Dr. Khalid Elyas Mohamed Elameen Alkhidir, Department of Petroleum and Natural Gas Engineering, College of Engineering, King Saud University, Saudi Arabia. E-mail id: kalkhidir@ksu.edu.sa

Received Date: Mar 05, 2020; **Accepted Date:** Mar 13, 2020; **Published Date:** Mar 16, 2020

Abstract

The quality and assessment of a reservoir can be documented in details by the application of seismo magentic power density. This research aims to calculate fractal dimension from the relationship among seismo magentic power density, maximum seismo magentic power density and wetting phase saturation and to approve it by the fractal dimension derived from the relationship among capillary pressure and wetting phase saturation. Two equations for calculating the fractal dimensions have been employed. The first one describes the functional relationship between wetting phase saturation, seismo magentic power density, maximum seismo magentic power density and fractal dimension. The second equation implies to the wetting phase saturation as a function of capillary pressure and the fractal dimension. Two procedures for obtaining the fractal dimension have been utilized. The first procedure was done by plotting the logarithm of the ratio between seismo magentic power density and maximum seismo magentic power density versus logarithm wetting phase saturation. The slope of the first procedure = 3- Df (fractal dimension). The second procedure for obtaining the fractal dimension was determined by plotting the logarithm of capillary pressure versus the logarithm of wetting phase saturation. The slope of the second procedure = Df -3. On the basis of the obtained results of the fabricated stratigraphic column and the attained values of the fractal dimension, the sandstones of the Shajara reservoirs of the Shajara Formation were divided here into three units

Keywords: Shajara reservoirs; Shajara formation; Seismo magentic power density fractal dimension; Capillary pressure fractal dimension monitoring; Technical and social robustness

Introduction

Seismo electric effects related to electro kinetic potential, dielectric permittivity, pressure gradient, fluid viscosity, and electric conductivity was first reported by [1]. Capillary pressure follows the scaling law at low wetting phase saturation was reported by [2]. Seismo electric phenomenon by considering electro kinetic coupling coefficient as a function of effective charge density, permeability, fluid viscosity and electric conductivity was reported by [3]. The magnitude of seismo electric current depends on porosity, pore size, zeta potential of the pore surfaces, and elastic properties of the matrix was investigated by [4]. The tangent of the ratio of converted electic field to pressure is approximately in inverse proportion to permeability was studied by [5]. Permeability inversion from seismoelectric log at low frequency was studied by [6]. They reported that, the tangent of the ratio among electric excitation intensity and pressure field is a function of porosity, fluid viscosity, frequency, tortuosity and fluid density and Dracy permeability. A decrease of seismo electric frequencies with increasing water content was reported by [7]. An increase of seismo electric transfer function with increasing water saturation was studied by [8]. An increase of dynamic seismo electric transfer function with decreasing fluid conductivity was described by [9]. The amplitude of seismo electric signal increases with increasing permeability which means that the seismo electric effects are directly related to the permeability and can be used to study the permeability of the reservoir was illustrated by [10]. Seismo electric coupling is frequency dependent and decreases expontialy when frequency increases was demonstrated by [11]. An increase of permeability with increasing seismo magnetic moment and seismo diffusion coefficient fractal dimension was reported by [12,13]. An increase of, molar enthalpy, work fractal, electro kinetic, bubble pressure and pressure head fractal dimensions with permeability increasing and grain size was described by [14-17].

Material and Method

Sandstone samples were collected from the surface type section of the Permo-Carboniferous Shajara Formation, latitude 26° 52' 17.4", longitude 43° 36' 18" (Figure1). Porosity was measured on collected samples using mercury intrusion Porosimetry and permeability was derived from capillary pressure data. The purpose of this paper is to obtain seismo magentic power density fractal dimension and to confirm it by capillary pressure fractal dimension. The fractal dimension of the first procedure is determined from the positive slope of the plot of logarithm of the ratio of seismo magentic power density to maximum seismo magentic power density log ($SMPD^{1/4}/SMPD^{1/4}_{max}$) versus log wetting phase saturation (logSw). Whereas the fractal dimension of the second procedure is determined from the negative slope of the plot of logarithm of log capillary pressure (log Pc) versus logarithm of wetting phase saturation (log Sw).

Citation: Khalid E M Elameen Alkhidir. On Similarity of Seismo Magentic Power Density and Capillary Pressure Fractal Dimension for Characterizing Shajara Reservoirs of the Permo-Carboniferous Shajara Formation, Saudi Arabia. Medcave J Environ Sci Technol. 2020; 2:104.

The Seismo magentic power density can be scaled as

$$Sw = \left[\frac{SMPD^{\frac{1}{4}}}{SMPD_{max}^{\frac{1}{4}}}\right]^{[3-Df]} \quad 1$$

Where Sw the water saturation, SMPD theseismo magentic power density in vott * second / square meter, SMPDmax the maximum seismo magentic power densityin vott * second / square meter, and Df the fractal dimension.

Equation 1 can be proofed from

$$H = \left[\frac{\phi * \epsilon * kf * \zeta * \rho f * SSWV * SRGV}{\alpha\infty * \eta}\right] \quad 2$$

Where H the magnetic field in ampere /meter, ϕ the porosity, ϵ the fluid permittivity in Faraday / meter, kf the fluid dielectric constant, the fluid densityPf in kilogram / cubic meter, SSWV the seismic shear wave velocity in meter / second, SRGV the seismoradial grain velocity in meter / second, α the tortuosity, η the fluid viscosity in pascal * second

The seismo magentic field H can be scaled as

$$H = \left[\frac{SEC}{d}\right] \quad 3$$

Where H the seismo magnetic field in ampere / meter, SEC the seismo electric current in ampere, and d the distance in meter

Insert equation 3 into equation 2

$$\left[\frac{SEC}{d}\right] = \left[\frac{\phi * \epsilon * kf * \zeta * \rho f * SSWV * SRGV}{\alpha\infty * \eta}\right] \quad 4$$

The seismo electric current SEC can be scaled as

$$SEC = \left[\frac{SEP}{R}\right] \quad 5$$

Where SEC the seismo electric current in ampere, SEP the seismo electric potential in volt, and R the resistance in ohm

Insert equation 5 into equation 4

$$\left[\frac{SEP}{d * R}\right] = \left[\frac{\phi * \epsilon * kf * \zeta * \rho f * SSWV * SRGV}{\alpha\infty * \eta}\right] \quad 6$$

The seismo electric potential can be scaled

$$SEP = \left[\frac{SMP}{ST}\right] \quad 7$$

Where SEP the seismo electric potential in volt, SMP the seismo magentic power in volt * second, ST the seismic time in second
Insert equation 7 into equation 6

$$\left[\frac{SMP}{d * R * ST}\right] = \left[\frac{\phi * \epsilon * kf * \zeta * \rho f * SSWV * SRGV}{\alpha\infty * \eta}\right] \qquad 8$$

The seismo magnetic power can be scaled as

$$SMP = SMPD * A \qquad 9$$

Where SMP the seismo magnetic power in volt * second, SMPD the seismo magentic power density in volt * second /square meter, and A the area in square meter

Insert equation 9 into equation 8

$$\left[\frac{SMPD * A}{d * R * ST}\right] = \left[\frac{\phi * \epsilon * kf * \zeta * \rho f * SSWV * SRGV}{\alpha\infty * \eta}\right] \qquad 10$$

The viscosity η can be scaled as

$$\eta = p * t \qquad 11$$

Where η the fluid viscosity in pascal * second, p the pressure in pascal, and t the time in second
Insert equation 11 into equation 12

$$\left[\frac{SMPD * A}{d * R * ST}\right] = \left[\frac{\phi * \epsilon * kf * \zeta * \rho f * SSWV * SRGV}{\alpha\infty * p * t}\right] \qquad 12$$

The time t can be scaled as

$$t = \left[\frac{V}{Q}\right] \qquad 13$$

Where t the time in second, V the volume in cubic meter, Q the flow rate in cubic meter / second
Insert equation 13 into equation 12

$$\left[\frac{SMPD * A}{d * R * ST}\right] = \left[\frac{\phi * \epsilon * kf * \zeta * \rho f * SSWV * SRGV * Q}{\alpha\infty * p * V}\right] \qquad 14$$

The flow rate can be scaled as

$$Q = \left[\frac{3.14 * r^4 * \Delta p}{8 * \eta * L}\right] \qquad 15$$

Where Q the flow rate in cubic meter / second, r the pore radius in meter, Δp the differential pressure in pascal, η the fluid viscosity in pascal * second, L the capillary length in meter.

Insert equation 15 into equation 14

$$\left[\frac{SMPD * A}{d * R * ST}\right] = \left[\frac{\phi * \epsilon * kf * \zeta * \rho f * SSWV * SRGV * 3.14 * r^4 * \Delta p}{\alpha\infty * p * V * 8 * \eta * L}\right] \quad 16$$

The maximum pore radius r_{max} can be scaled as

$$\left[\frac{SMPD_{max} * A}{d * R * ST}\right] = \left[\frac{\phi * \epsilon * kf * \zeta * \rho f * SSWV * SRGV * 3.14 * r_{max}^4 * \Delta p}{\alpha\infty * p * V * 8 * \eta * L}\right] \quad 17$$

Divide equation 16 by equation 17

$$\left[\frac{\left[\frac{SMPD * A}{d * R * ST}\right]}{\left[\frac{SMPD_{max} * A}{d * R * ST}\right]}\right] = \left[\frac{\left[\frac{\phi * \epsilon * kf * \zeta * \rho f * SSWV * SRGV * 3.14 * r^4 * \Delta p}{\alpha\infty * p * V * 8 * \eta * L}\right]}{\left[\frac{\phi * \epsilon * kf * \zeta * \rho f * SSWV * SRGV * 3.14 * r_{max}^4 * \Delta p}{\alpha\infty * p * V * 8 * \eta * L}\right]}\right] \quad 18$$

Equation 18 after simplification will become

$$\left[\frac{SMPD}{SMPD_{max}}\right] = \left[\frac{r^4}{r_{max}^4}\right] \quad 19$$

Take the fourth root of equation 19

$$\sqrt[4]{\left[\frac{SMPD}{SMPD_{max}}\right]} = \sqrt[4]{\left[\frac{r^4}{r_{max}^4}\right]} \quad 20$$

Equation 20 after simplification will become

$$\left[\frac{SMPD^{\frac{1}{4}}}{SMPD_{max}^{\frac{1}{4}}}\right] = \left[\frac{r}{r_{max}}\right] \quad 21$$

Take the logarithm of equation 21

$$\log\left[\frac{SMPD^{\frac{1}{4}}}{SMPD_{max}^{\frac{1}{4}}}\right] = \log\left[\frac{r}{r_{max}}\right] \quad 22$$

$$\text{But; } \log\left[\frac{r}{r_{max}}\right] = \left[\frac{\log Sw}{3 - Df}\right] \quad 23$$

Insert equation 23 into equation 22

$$\left[\frac{\log Sw}{3 - Df}\right] = \log\left[\frac{SMPD^{\frac{1}{4}}}{SMPD_{max}^{\frac{1}{4}}}\right] \quad 24$$

Equation 24 after log removal will become

$$Sw = \left[\frac{SMPD^{\frac{1}{4}}}{SMPD_{max}^{\frac{1}{4}}}\right]^{[3-Df]} \quad 25$$

Equation 25 the proof of equation 1 which relates the water saturation, seismo magentic power density, maximum seismo magentic power density, and the fractal dimension.
The capillary pressure can be scaled as

$$LogSw = [Df - 3] * \log pc + constant \quad 26$$

Where Sw the water saturation, Pc the capillary pressure and Df the fractal dimension.

Results and Discussion

Based on field observation the Shajara Reservoirs of the Permo-Carboniferous Shajara Formation were divided here into three units as described in (Figure 1). These units from bottom to top are: Lower Shajara Reservoir, Middle Shajara reservoir, and Upper Shajara Reservoir. Their attained results of the seismo magentic power density fractal dimension and capillary pressure fractal dimension are shown in (Table 1). Based on the achieved results it was found that the seismo magentic power density fractal dimension is equal to the capillary pressure fractal dimension. The maximum value of the fractal dimension was found to be 2.7872 allocated to sample SJ13 from the Upper Shajara Reservoir as verified in (Table 1). Whereas the minimum value of the fractal dimension 2.4379 was reported from sample SJ3 from the Lower Shajara reservoir as shown in (Table 1). The Seismo magentic power density fractal dimension and capillary pressure fractal dimension were detected to increase with increasing permeability as proofed in owing to the possibility of having interconnected channels (Table 1).

The Lower Shajara reservoir was symbolized by six sandstone samples (Figure 1), four of which label as SJ1, SJ2, SJ3 and SJ4 were carefully chosen for capillary pressure measurement as proven in (Table 1). Their positive slopes of the first procedure log of the Seismo magentic power density to maximum Seismo magentic power density versus log wetting phase saturation (Sw) and negative slopes of the second procedure log capillary pressure (Pc) versus log wetting phase saturation (Sw) are clarified in (Figure 2- 5 and Table 1). Their Seismo magentic power density fractal dimension and capillary pressure fractal dimension values are revealed in (Table 1). As we proceed from sample SJ2 to SJ3 a pronounced reduction in permeability due to compaction was described from 1955 md to 56 md which reflects decrease in Seismo magentic power density fractal dimension from 2.7748 to 2.4379 as quantified in (Table 1). Again, an increase in grain size and permeability was proved from sample SJ4 whose seismo magentic power density fractal dimension and capillary pressure fractal dimension was found to be 2.6843 as described in (Table 1).

In contrast, the Middle Shajara reservoir which is separated from the Lower Shajara reservoir by an unconformity surface as revealed in (Figure 1). It was nominated by four samples (Figure 1), three of which named as SJ7, SJ8, and SJ9 as illuminated in were chosen for capillary measurements as described in (Table 1). Their positive slopes of the first procedure and negative slopes of the second procedure are shown in (Figure 6-8 and Table 1). Furthermore, their Seismo magentic power density fractal dimensions and capillary pressure fractal dimensions show similarities as defined in (Table 1). Their fractal dimensions are higher than those of samples SJ3 and SJ4 from the Lower Shajara Reservoir due to an increase in their permeability as explained in (Table 1).

On the other hand, the Upper Shajara reservoir was separated from the Middle Shajara reservoir by yellow green mudstone as shown in (Figure 1). It is defined by three samples so called

SJ11, SJ12, SJ13 as explained in (Table 1). Their positive slopes of the first procedure and negative slopes of the second procedure are displayed in (Figure 9-11 and Table 1). Moreover, their seismo magentic power density fractal dimension and capillary pressure fractal dimension are also higher than those of sample SJ3 and SJ4 from the Lower Shajara Reservoir due to an increase in their permeability as simplified in (Table 1).

Overall a plot of positive slope of the first procedure versus negative slope of the second procedure as described in reveals three permeable zones of varying Petrophysical properties (Figure 12). These reservoir zones were also confirmed by plotting seismo magentic power density fractal dimension versus capillary pressure fractal dimension as described in (Figure 13). Such variation in fractal dimension can account for heterogeneity which is a key parameter in reservoir quality assessment.

Conclusion

The sandstones of the Shajara Reservoirs of the permo-Carboniferous Shajara Formation were divided here into three units based on seismo magentic power density fractal dimension.The Units from base to top are: Lower Shajara Seismo Magnetic Power DensityFractal Dimension Unit, Middle Shajara Seismo Magnetic Power Density Fractal Dimension Unit, and Upper Shajara Seismo Magnetic Power Density Fractal Dimension Unit. These units were also proved by capillary pressure fractal dimension. The fractal dimension was found to increase with increasing grain size and permeability owing to possibility of having interconnected channels.

Formation	Reservoir	Sample	Porosity %	k (md)	Positive slope of the first procedure Slope=3-Df	Negative slope of the second procedure Slope=Df-3	Seismo magentic power densityfractal dimension	Capillary pressure fractal dimension
Permo-Carboniferous Shajara Formation	Upper Shajara Reservoir	SJ13	25	973	0.2128	-0.2128	2.7872	2.7872
		SJ12	28	1440	0.2141	-0.2141	2.7859	2.7859
		SJ11	36	1197	0.2414	-0.2414	2.7586	2.7586
	Middle Shajara Reservoir	SJ9	31	1394	0.2214	-0.2214	2.7786	2.7786
		SJ8	32	1344	0.2248	-0.2248	2.7752	2.7752
		SJ7	35	1472	0.2317	-0.2317	2.7683	2.7683
	Lower Shajara Reservoir	SJ4	30	176	0.3157	-0.3157	2.6843	2.6843
		SJ3	34	56	0.5621	-0.5621	2.4379	2.4379
		SJ2	35	1955	0.2252	-0.2252	2.7748	2.7748
		SJ1	29	1680	0.2141	-0.2141	2.7859	2.7859

Table 1: Petrophysical model showing the three Shajara Reservoir Units with their corresponding values of seismo magentic power density fractal dimension and capillary pressure fractal dimension.

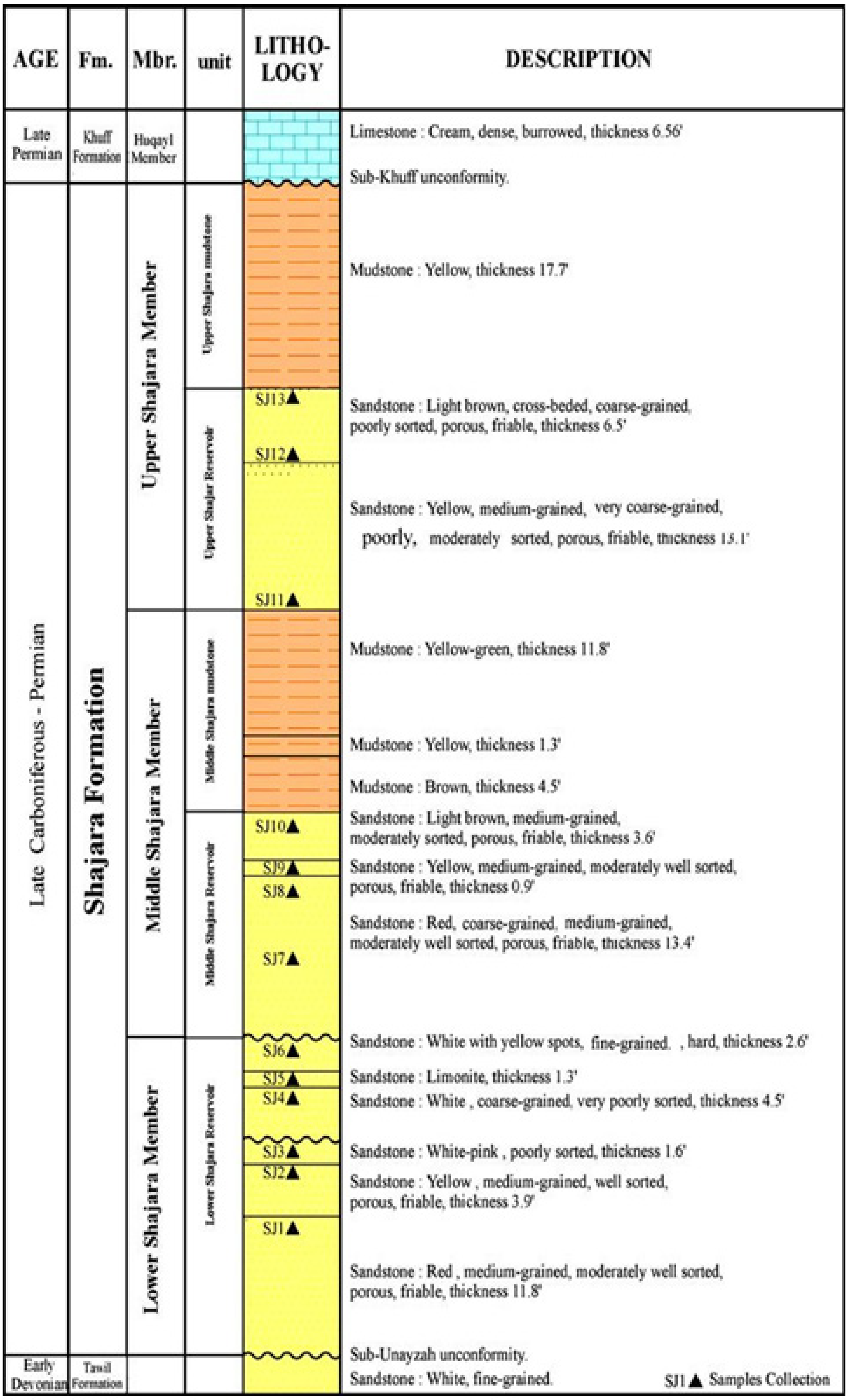

Figure 1: Surface type section of the Shajara Reservoirs of the Permo-Carboniferous Shajara Formation at latitude 26° 52' 17.4" longitude 43° 36' 18".

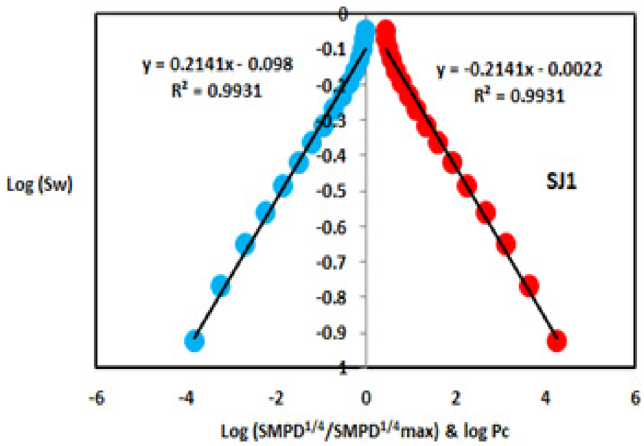

Figure 2: Log ($SMPD^{1/4}$/$SMPD^{1/4}_{max}$) & log pc versus log Sw for sample SJ1

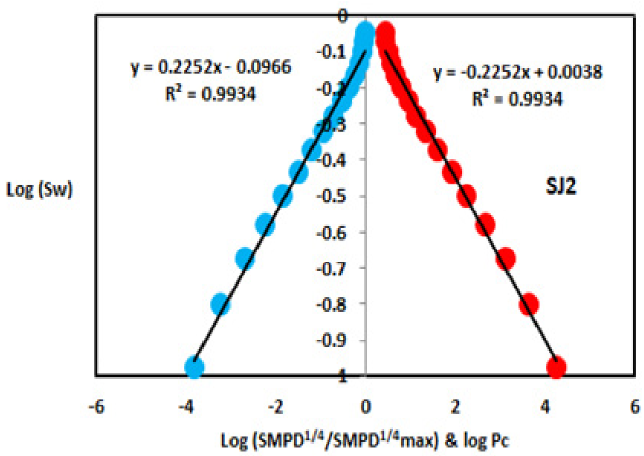

Figure 3: Log ($SMPD^{1/4}$/$SMPD^{1/4}_{max}$) & log pc versus log Sw for sample SJ2.

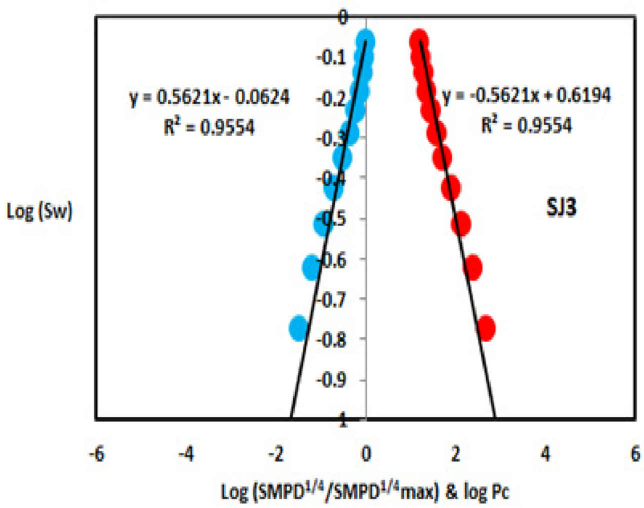

Figure 4: Log ($SMPD^{1/4}$/$SMPD^{1/4}_{max}$) & log pc versus log Sw for sample SJ3.

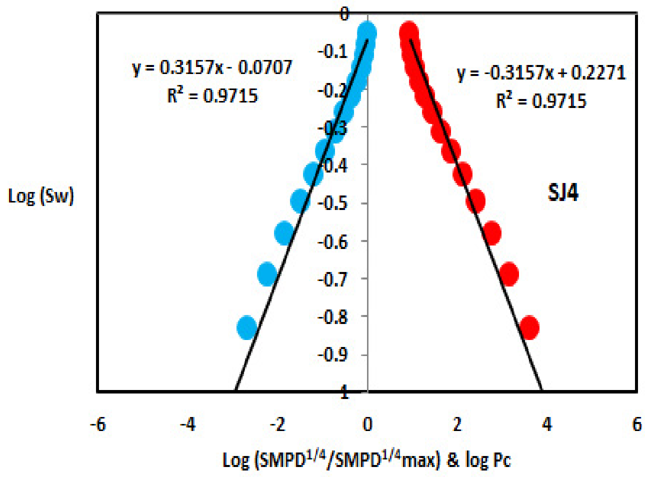

Figure 5: Log ($SMPD^{1/4}$/$SMPD^{1/4}_{max}$) & log pc versus log Sw for sample SJ4.

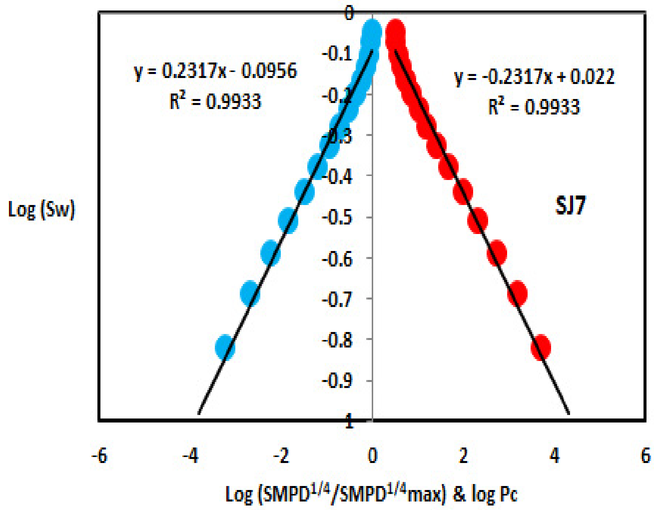

Figure 6: Log ($SMPD^{1/4}$/$SMPD^{1/4}_{max}$) & log pc versus log Sw for sample SJ7.

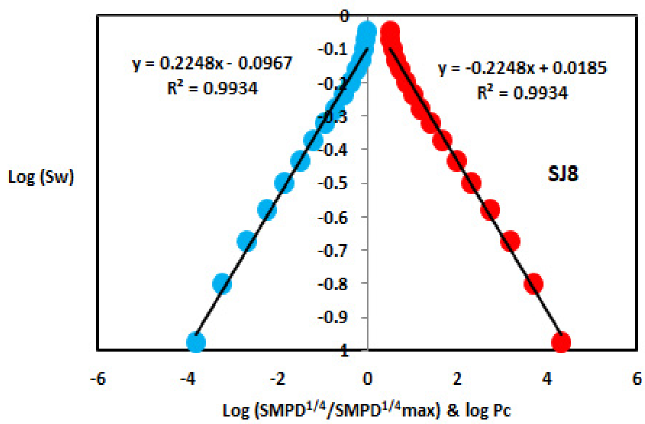

Figure 7: Log ($SMPD^{1/4}$/$SMPD^{1/4}_{max}$) & log pc versus log Sw for sample SJ8.

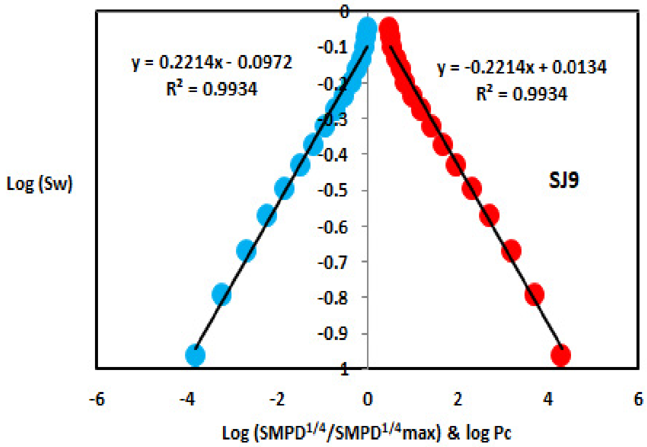

Figure 8: Log ($SMPD^{1/4}/SMPD^{1/4}{}_{max}$) & log pc versus log Sw for sample SJ9.

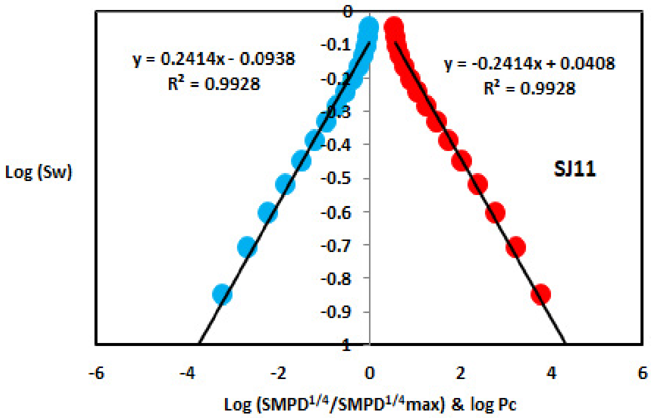

Figure 9: Log ($SRGV^{1/4}/SRGV^{1/4}{}_{max}$) & log pc versus log Sw for sample SJ11.

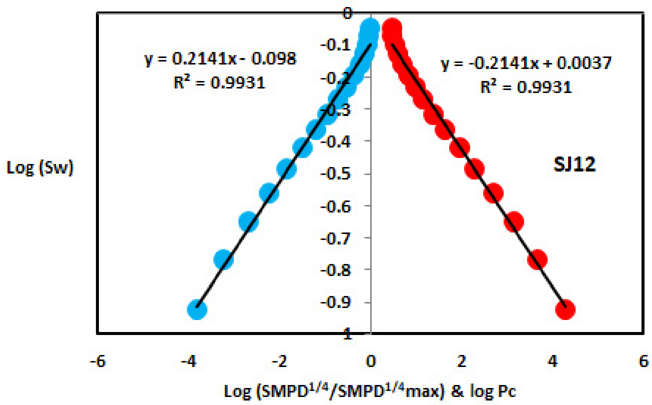

Figure 10: Log ($SMPD^{1/4}/SMPD^{1/4}{}_{max}$) & log pc versus log Sw for sample SJ12.

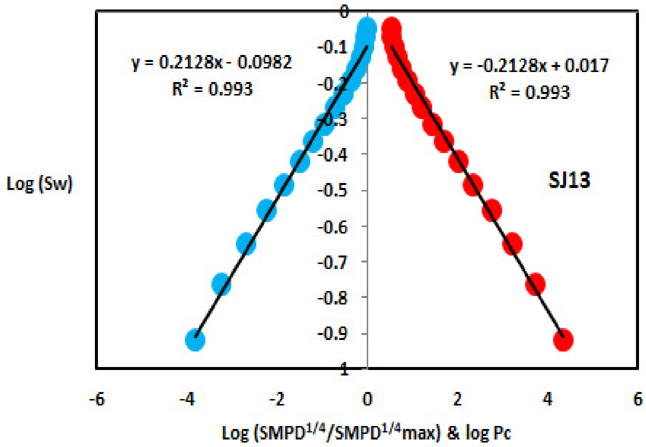

Figure 11: Log ($SMPD^{1/4}/SMPD^{1/4}{}_{max}$) & log pc versus log Sw for sample SJ13.

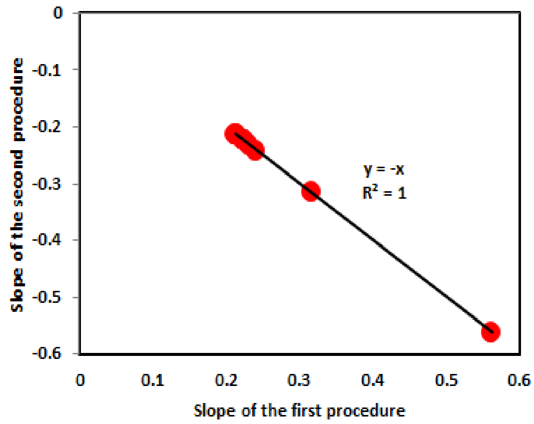

Figure 12: Slope of the first procedure versus slope of the second procedure.

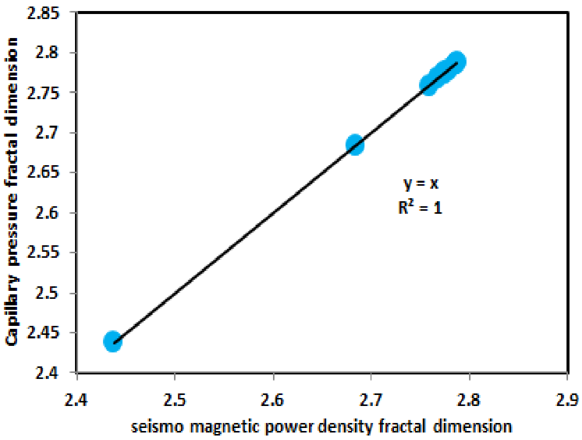

Figure 13: Seismo magentic power density fractal dimension versus capillary pressure fractal dimension.

Acknowledgement

The author would to thank King Saud University, college of Engineering, Department of Petroleum and Natural Gas Engineering, Department of Chemical Engineering, Research Centre at College of Engineering, College of science, Department of Geology, and King Abdullah Institute for research and Consulting Studies for their supports.

References

1. Frenkel J. On the theory of seismic and seismoelectric phenomena in a moist soil. Journal of physics. 1944; 3: 230-241.
2. Li K, Williams W. Determination of capillary pressure function from resistivity data. Transport in Porous Media. 2007; 67: 1-15.
3. Revil A, Jardani A. Seismo electric response of heavy oil reservoirs: theory and numerical modelling. Geophysical J International. 2020; 180: 781-797.
4. Dukhin A, Goetz P, Thommes M. Seismoelectric effect: a non-isochoric streaming current.1 Experiment. J Colloid Interface Sci. 2020; 345: 547-553.
5. Guan W, Hu H, Wang Z. Permeability inversion from low-frequency seismoelectric logs in fluid- saturated porous formations. Geophys Prospect. 2012; 61: 120-133.
6. Hu H, Guan W, Zhao W. Theoretical studies of permeability inversion from seismoelectric logs. Geophysical Research Abstracts. 2012; 14: EGU2012-6725-1 2012 EGU General Assembly.
7. Borde C, S en echal P Barri`ere J, Brito D, Normandin E, et al. Impact of water saturation on seismoelectric transfer functions: a laboratory study of co-seismic phenomenon. Geophysical J International. 2015; 200: 1317-1335.
8. Jardani A, Revil A. Seismoelectric couplings in a poroelastic material containing two immiscible fluid phases. Geophysical Journal International. 2015; 202: 850-870.
9. Holzhauer J, Brito D, Bordes C, Brun Y, Guatarbes B. Experimental quantification of the seismoelectric transfer function and its dependence on conductivity and saturation in loose sand. Geophys Prospect. 2016; 65: 1097-1120
10. Rong Peng, Jian-Xing Wei, Bang-Rang Di, Pin-Bo Ding, ZiChun Liu Experimental research on seismoelectric effects in sandstone. Applied Geophysics. 2016; 13: 425-436.
11. Djuraev U, Jufar S R, Vasant P. Numerical Study of frequency-dependent seismo electric coupling in partiallysaturated porous media. 2017 MATEC Web of Conferences. 87: 02001.
12. Alkhidir KEME. Seismo Magnetic Moment Fractal Dimension for Characterizing Shajara Reservoirs of the Permo-Carboniferous Shajara Formation, Saudi Arabia World Scientific News. 2020; 139: 186-200.
13. Alkhidir KEME. Seismo Diffusion Coefficient Fractal Dimension for Characterizing Shajara Reservoirs of the Permo-Carboniferous Shajara Formation, Saudi Arabia. Research Journal of Nanoscience and Engineering. 2019; 3: 23-29.
14. Alkhidir KEME. Molar Enthalpy Fractal Dimension for Characterizing Shajara Reservoirs of the Permo-Carboniferous Shajara Formation. Journal of Agriculture and Aquaculture. 2019; 1: 1-8.
15. Alkhidir KEME. Work Fractal Dimension for Characterizing Shajara Reservoirs of the PermoCarboniferous Shajara Formation, Saudi Arabia. Int J Environ & Agri Sci. 2019; 3: 1-8
16. Alkhidir KEME. Electro Kinetic Fractal Dimension for Characterizing Shajara Reservoirs of the Shajara Formation. Int J Nano Med & Eng. 2018; 3: 54-60.
17. Al-Khidir KE. On Similarity of Pressure Head and Bubble Pressure Fractal Dimensions for Characterizing Permo-Carboniferous Shajara Formation, Saudi Arabia. J Indust Pollut Toxic. 2018; 1: 102.